Supplement of Biogeosciences, 19, 1277–1301, 2022
https://doi.org/10.5194/bg-19-1277-2022-supplement

Biogeosciences
Open Access

Supplement of

Marine CO_2 system variability along the northeast Pacific Inside Passage determined from an Alaskan ferry

Wiley Evans et al.

Correspondence to: Wiley Evans (wiley.evans@hakai.org)

Supplemental Text S1: M/V *Columbia* schedule

The vessel left Bellingham, WA (Figure 1) on Friday evening and arrived in Ketchikan, AK by Sunday morning. From there, the ship travelled north to Wrangell, Petersburg, Juneau, Haines, and Skagway. After leaving Skagway, the M/V *Columbia* travelled south to Sitka, then back to Ketchikan by Wednesday afternoon, and finally returned to Bellingham, WA by Friday morning.

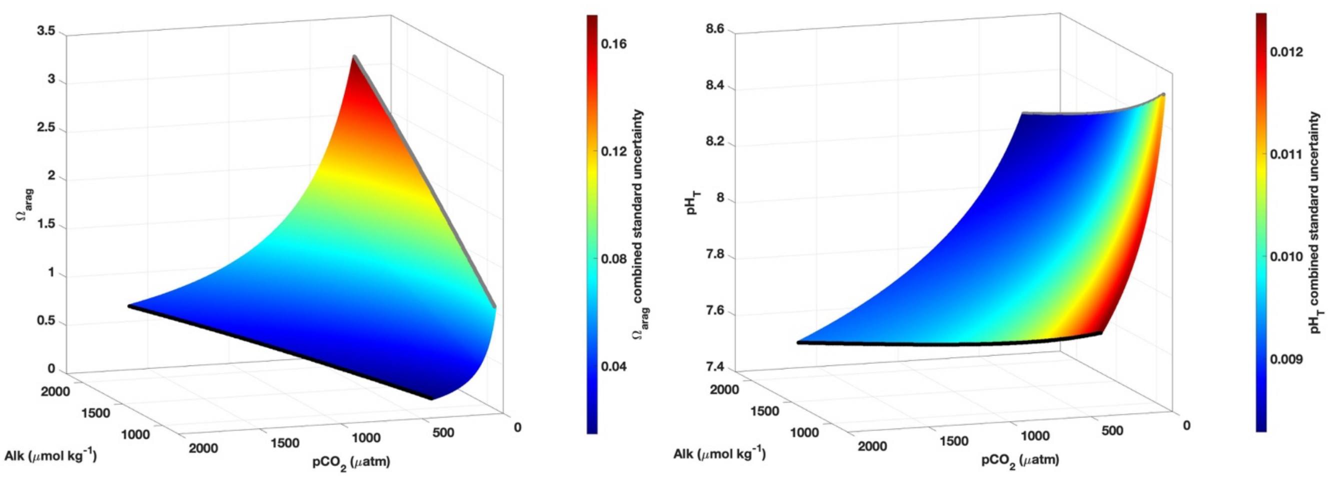

Supplemental Figure S1: Combined standard uncertainty in Ω_{arag} (left) and pH_T (right) as a function of pCO_2 (μatm) and alkalinity (Alk; μmol kg^{-1}). pCO_2 is computed across a range of TCO_2:Alk ratios in each panel, with the grey line equalling a ratio of 0.85 and the black line being unity.

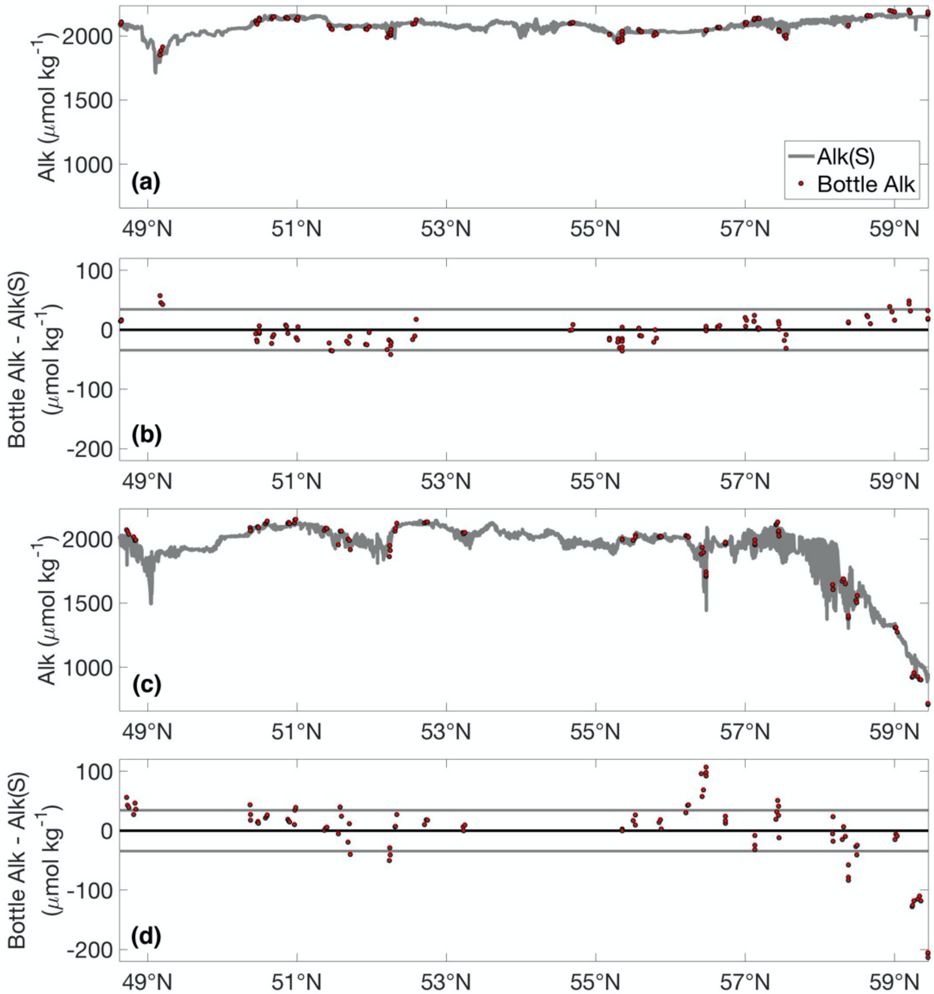

Supplemental Figure S2: Comparison between estimated and derived alkalinity (Alk) from two ferry ride-along cruises between November 11 to 17, 2017 and August 25 to 31, 2018. Panel a shows Alk estimated using the Alk-salinity relationship from Evans et al. (2015) (grey line; Alk(S)) and Alk calculated from discrete pCO_2 and TCO_2 measurements (red circles; Bottle Alk) from the first cruise in November 2017. Panel b is Bottle Alk minus Alk(S), with the grey horizontal lines as two times the RMSE of the Evans et al. (2015) relationship (34 μmol kg^{-1}). Panel c shows Alk(S) and Bottle Alk from the second ride-along cruise in August 2018, with Panel d is the difference in these parameters. Alk is over-estimated by ~200 μmol kg^{-1} during the summer melt season in the region of lowest alkalinity along the northern portion of the transit.

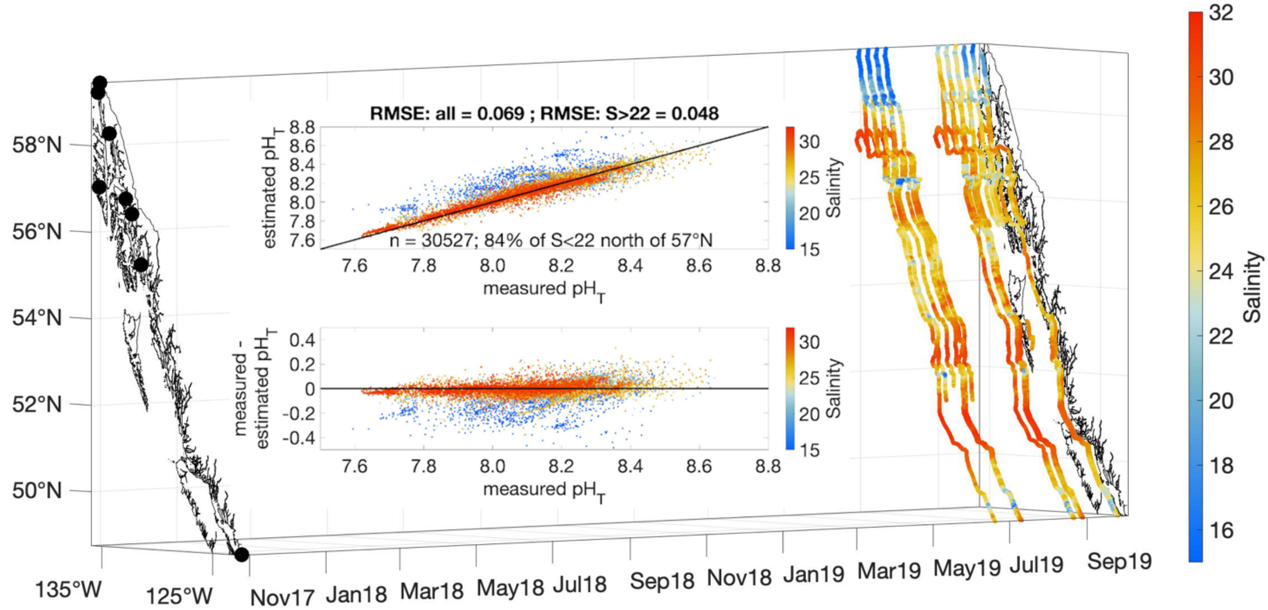

Supplemental Figure S3: Map shows the distribution of salinity measurements that correspond to BGC-SUMO pH_T data used to fill missing pCO_2 observations. The insert shows the comparison between BGC-SUMO pH_T and pH_T estimated from pCO_2 and the regional Alk-salinity relationship. Total number of comparison points was 30527 measurements. RMSE between measured and estimated pH_T was 0.069, and decreased to 0.048 for seawater measurements with S > 22. The largest offset between directly measured and estimated pH_T was in seawater with S < 22. 84% of S < 22 seawater was observed north of 57°N during summer months in the region around Juneau and in Lynn Canal. In this region, the estimated Alk was too high, which resulted in pH_T and Ω_{arag} being over-estimated and pCO_2 being under-estimated for instances where pH_T was used to fill missing observations in low S water. However, the region still maintained $\Omega_{arag} < 1$, so accounting for this over-estimation would lead to more corrosive conditions. X- and y-axes represent longitude and latitude, respectively, and with the coastline and terminal positions shown as in Figure 1 and time increasing along the z-axis.

Supplemental Text S2: Assessment of Seasonal Drivers

The basis for assessing seasonal drivers stems from the following thermodynamic relationship from Takahashi et al. (1993):

$$\Delta pCO_2 = \left({\partial pCO_2}/{\partial T} \right) \Delta T + \left({\partial pCO_2}/{\partial TCO_2} \right) \Delta TCO_2 + \left({\partial pCO_2}/{\partial TALK} \right) \Delta TALK + \left({\partial pCO_2}/{\partial S} \right) \Delta S \qquad \text{(Equation 1)}$$

that defines the change in pCO_2 in seawater as a function of variation in temperature (T), TCO_2, total alkalinity (TALK, taken here to equal Alk when organic acid contributions are negligible), and salinity (S). Each partial differential term represents a "buffer factor", with the two most commonly discussed in the literature being the Revelle factor (Sundquist et al., 1979;Egleston et al., 2010;Middelburg et al., 2020), $\left({\partial \ln pCO_2}/{\partial \ln TCO_2} \right)$, and the temperature sensitivity (Takahashi et al., 1993;Takahashi et al., 2002), $\left({\partial \ln pCO_2}/{\partial T} \right)$. The global average Revelle factor is 10, meaning a 10% change in pCO_2 would result from a 1% change in TCO_2; whereas the temperature sensitivity of pCO_2 is 0.0423, meaning pCO_2 changes by roughly 4% per degree temperature change. Processes that drive variation in these four terms are seasonal warming and cooling, freshening and evaporation, physical transport and mixing, net community production (primary production minus community respiration), sea-air CO_2 exchange, and calcification. The first two processes listed are thermodynamic drivers, and the remaining processes are biophysical drivers. In most open ocean applications, seasonal variation in pCO_2 is dominated by variation in temperature and TCO_2 (Takahashi et al., 2002). Removing the temperature component (pCO_2 T-component) of the variability from the observations leaves behind variability driven by the remaining three terms in Equation 1. pCO_2 variability with the pCO_2 T-component removed is expressed as:

$$pCO_2 \text{ at } T_{mean} = pCO_{2,obs} \times e^{0.0423(T_{mean} - T_{Obs})} \qquad \text{(Equation 2)}$$

where T_{mean} is the mean temperature, and $pCO_{2,obs}$ and T_{obs} are the pCO_2 and temperature (T) observations within a grid cell. The pCO_2 T-component of seawater pCO_2 variability can be determined as the difference between the observations and pCO_2 at T_{mean}. Here, the salinity component was computed using the relationship from Sarmiento and Gruber (2006) derived from Equation 1:

$$pCO_2 \text{ S} - \text{component} = \Delta S \times \left({\overline{pCO_2}}/{\overline{S}} \right) \times \left(\gamma_S + \gamma_{TCO2} + \gamma_{TALK} \right) \qquad \text{(Equation 3)}$$

that importantly captures the impact of changing salinity on not just pCO_2 sensitivity (the last term in Equation 1) but also TCO_2 and Alk. This was done using mean pCO_2 and salinity (S) in each grid cell, defined as $\overline{pCO_2}$ and $\overline{S}$, with the salinity (γ_S), TCO_2 (γ_{TCO2}), and TALK (γ_{TALK}) buffer factors (Takahashi et al., 1993). We used global average values for these three buffer factors in this computation. The values were 1, 10, and -9.4 for γ_S, γ_{TCO2}, and γ_{TALK}, respectively (Takahashi et al., 1993). Note that γ_{TCO2} and γ_{TALK} oppose each other, and differences from the global averages would be largely compensated for by the competing influence of increasing (or decreasing) TCO_2 and increasing (or decreasing) Alk. Finally, the thermodynamic components, pCO_2 T-component and pCO_2 S-component, can be combined and then differenced from the observations to isolate variability that results from the remaining biophysical drivers. The seasonal amplitude of each component of pCO_2 variability was assessed, and the ratio of the amplitude of thermodynamic (T, S, or TS) to biophysical drivers (B_T, B_S, B_{TS}; where subscript denotes the removed terms) defined which was more important for determining pCO_2 variability on an annual basis (Takahashi et al., 2002;Fassbender et al., 2018).

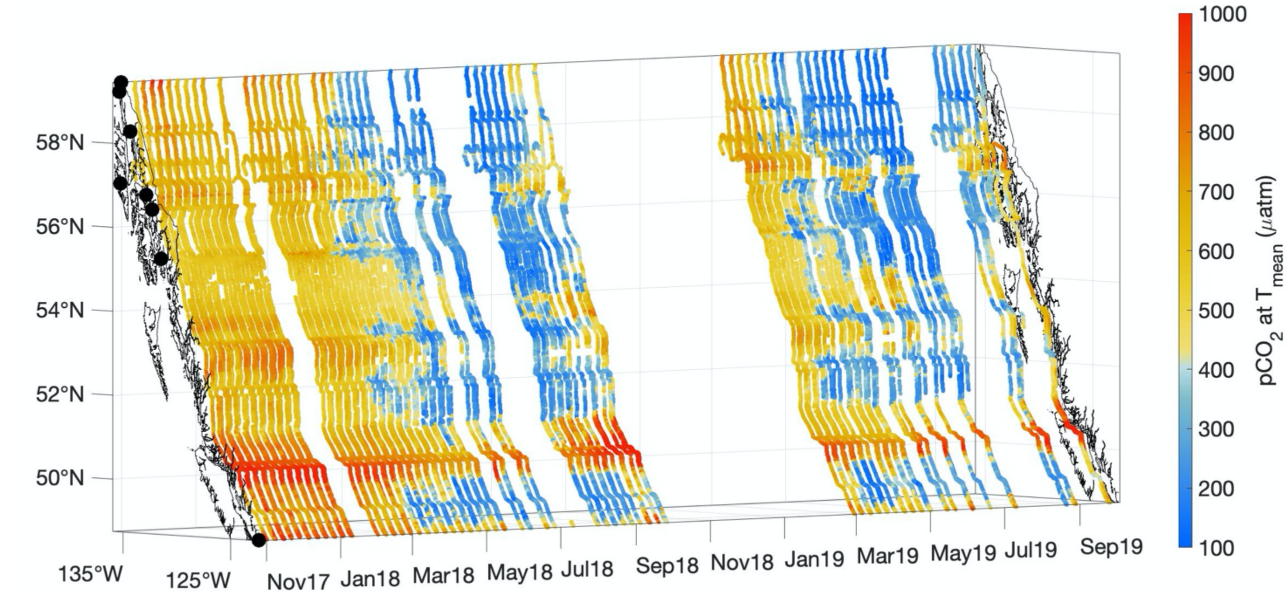

Supplemental Figure S4: The biophysical component of pCO_2 variability (µatm). X- and y-axes represent longitude and latitude, respectively, and with the coastline and terminal positions shown as in Figure 1 and time increasing along the z-axis.

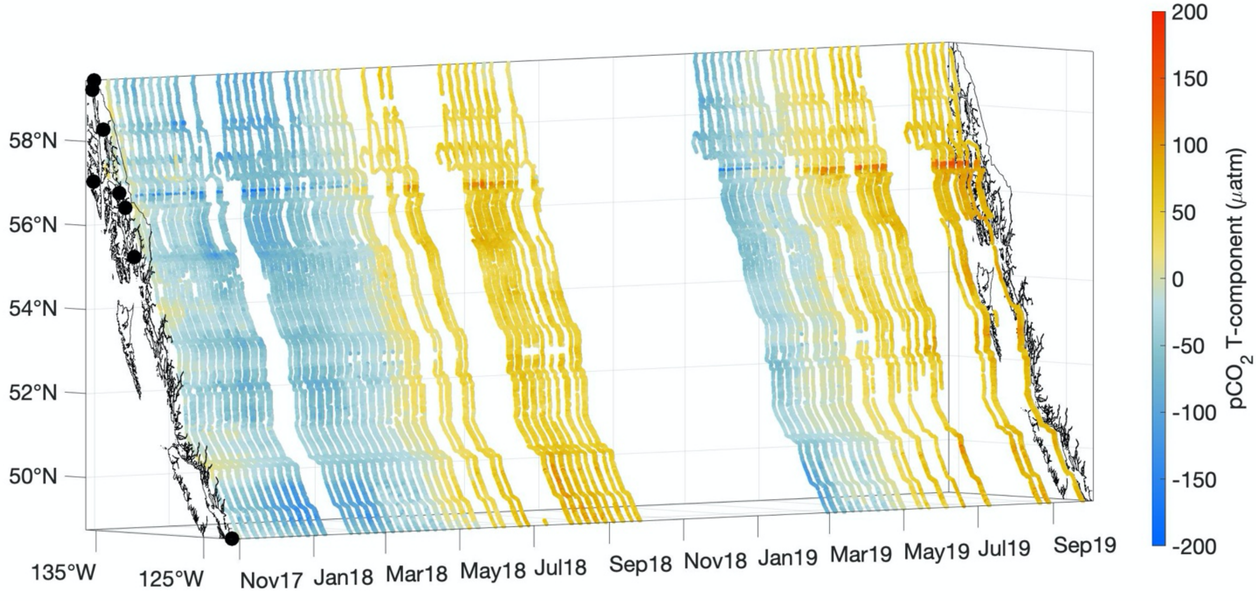

Supplemental Figure S5: The temperature component of pCO_2 variability (µatm). X- and y-axes represent longitude and latitude, respectively, and with the coastline and terminal positions shown as in Figure 1 and time increasing along the z-axis.

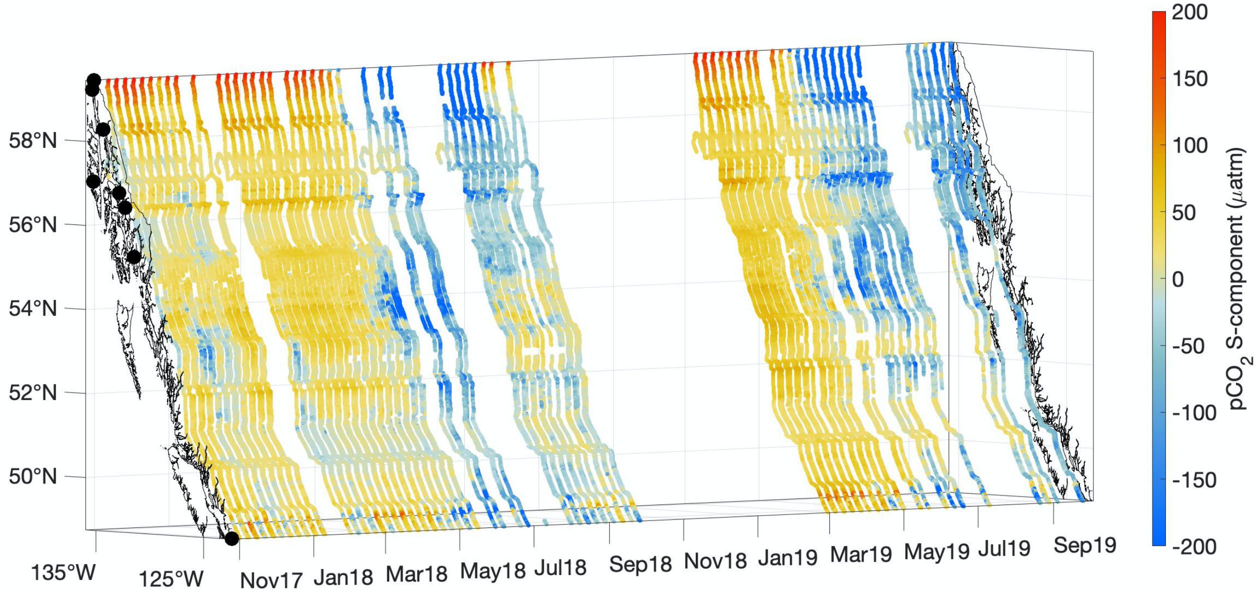

Supplemental Figure S6: The salinity component of pCO_2 variability (μatm). X- and y-axes represent longitude and latitude, respectively, and with the coastline and terminal positions shown as in Figure 1 and time increasing along the z-axis.

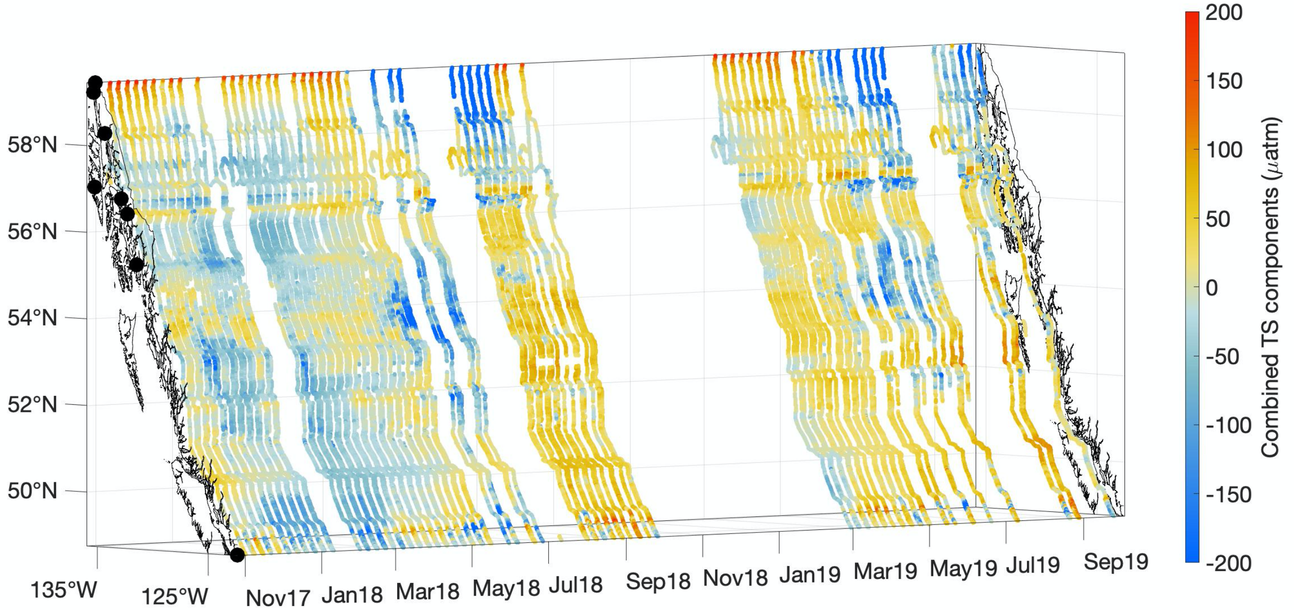

120 **Supplemental Figure S7:** The combined temperature and salinity components of pCO_2 variability (µatm). X- and y-axes represent longitude and latitude, respectively, and with the coastline and terminal positions shown as in Figure 1 and time increasing along the z-axis.

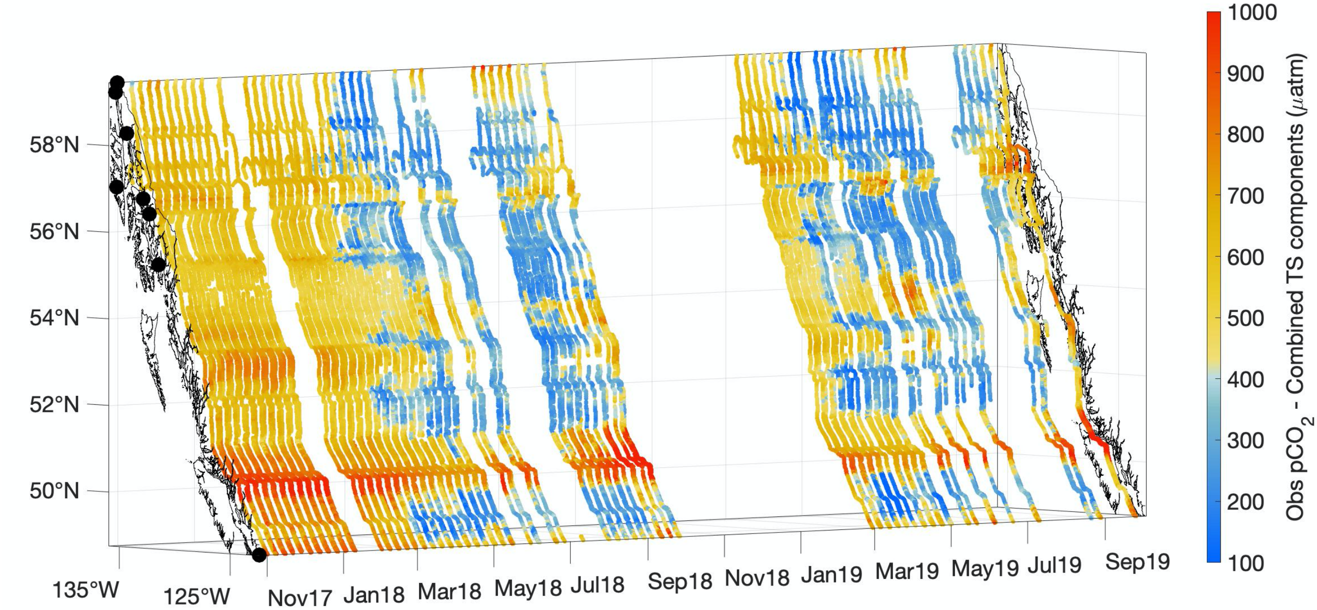

Supplemental Figure S8: Observed pCO_2 minus the combined temperature and salinity components of pCO_2 variability (µatm). Subtracting both the pCO_2 S-component and the pCO_2 T-component (TS) from the observed pCO_2 leaves remaining variability associated mainly with NCP because calcification is only episodically important in this region and gas exchange is slow (order months). X- and y-axes represent longitude and latitude, respectively, and with the coastline and terminal positions shown as in Figure 1 and time increasing along the z-axis.

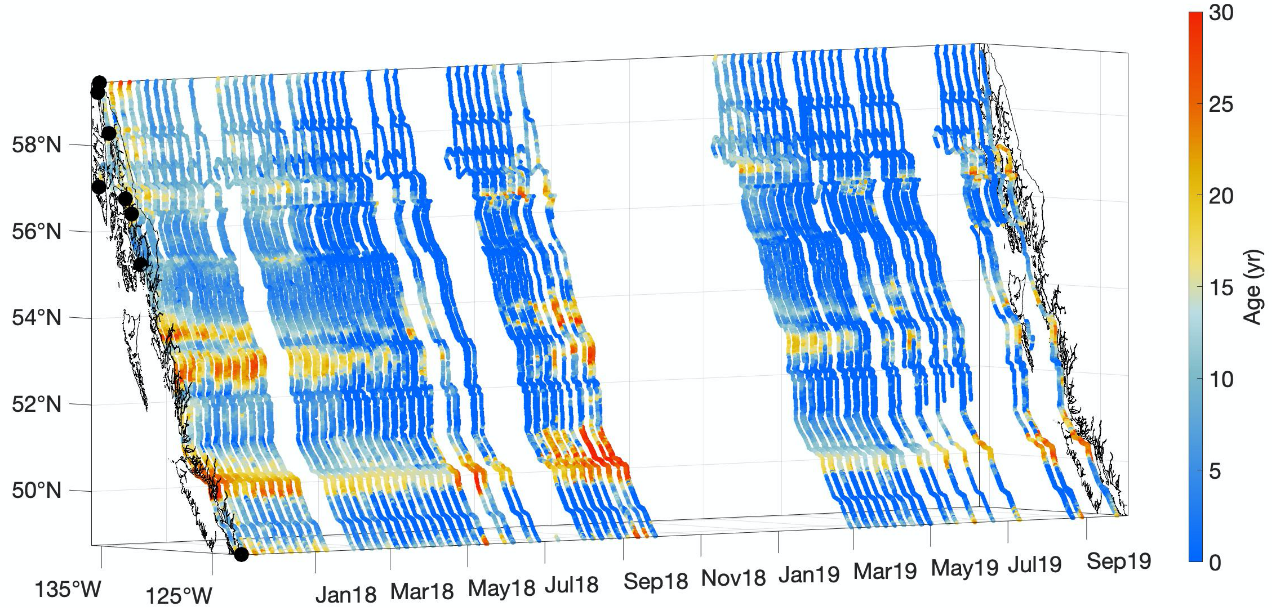

135 **Supplemental Figure S9:** The age (yr), or time since last contact with the atmosphere, of surface water along the Inside Passage. X- and y-axes represent longitude and latitude, respectively, and with the coastline and terminal positions shown as in Figure 1 and time increasing along the z-axis.

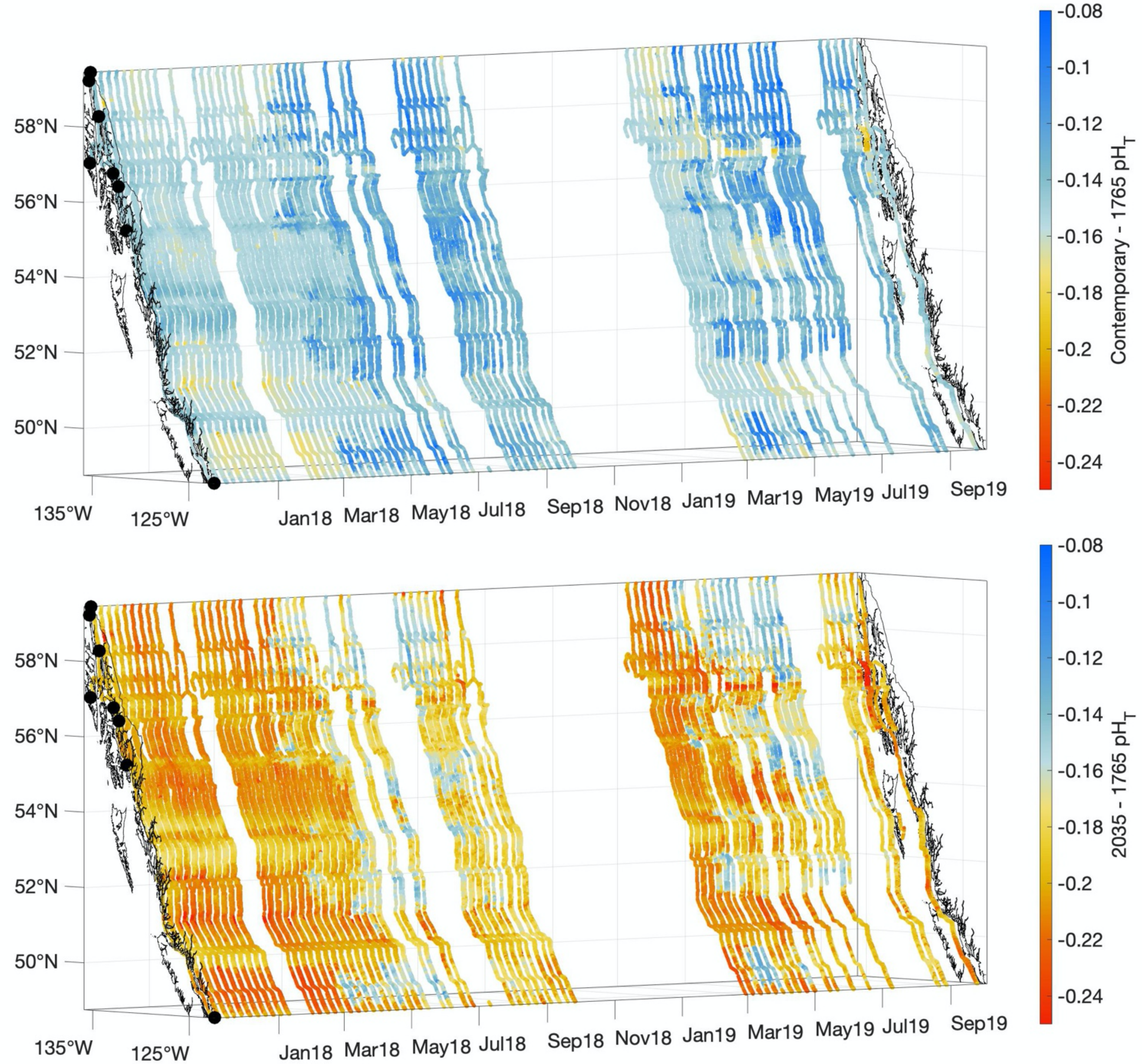

Supplemental Supplementary Figure S10: The contemporary pH$_T$ values minus the estimated values for 1765 (top) and the estimated values for 2035 minus the 1765 values (bottom). X- and y-axes represent longitude and latitude, respectively, and with the coastline and terminal positions shown as in Figure 1 and time increasing along the z-axis.

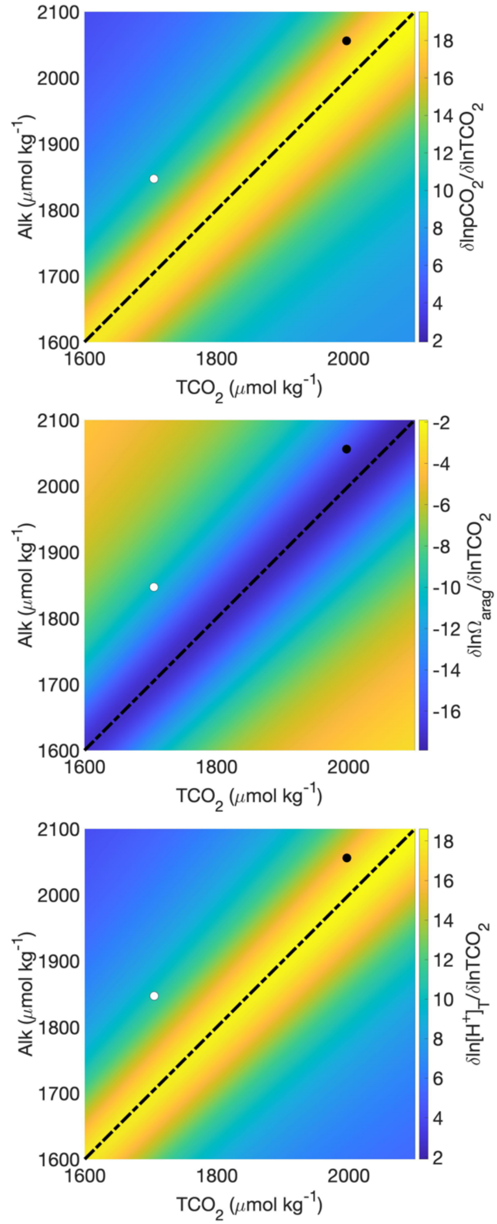

Supplemental Figure S11: Buffer factors for pCO_2 (top, the Revelle factor), Ω_{arag} (middle), and $[H^+]_T$ (bottom) as a function of TCO_2 and Alk. The buffer factor is the percentage change in each variable following a percentage change in TCO_2. The dashed line denotes equal TCO_2 and Alk across the range of values shown, and is the minimum buffering state (and maximum Revelle factor) for all buffer factors. Average TCO_2 and Alk values for summer (white circle) and winter (black circle) are shown to highlight that winter conditions on average are closer to the minimum buffering state, and therefore percentage changes in these values will be greatest during winter.

References

Egleston, E. S., Sabine, C. L., and Morel, F. M. M.: Revelle revisited: Buffer factors that quantify the response of ocean chemistry to changes in DIC and alkalinity, Global Biogeochemical Cycles, 24, doi: 10.1029/2008GB003407, 2010.

Evans, W., Mathis, J. T., Ramsay, J., and Hetrick, J.: On the Frontline: Tracking Ocean Acidification in an Alaskan Shellfish Hatchery, PLoS One, 10, e0130384, 10.1371/journal.pone.0130384, 2015.

Fassbender, A. J., Rodgers, K. B., Palevsky, H. I., and Sabine, C. L.: Seasonal Asymmetry in the Evolution of Surface Ocean pCO_2 and pH Thermodynamic Drivers and the Influence of Sea-Air CO_2 Flux, Global Biogeochemical Cycles, 32, 1476-1497, 2018.

Middelburg, J. J., Soetaert, K., and Hagens, M.: Ocean Alkalinity, Buffering and Biogeochemical Processes, Reviews of Geophysics, doi.org/10.1029/2019RG000681, 2020.

Sarmiento, J. L., and Gruber, N.: Ocean Biogeochemical Dynamics, Princeton University Press, Princeton, 2006.

Sundquist, E. T., Plummer, L. N., and Wigley, T. M. L.: Carbon Dioxide in the Ocean Surface: The Homogeneous Buffer Factor, Science, 204, 1203-1205, 1979.

Takahashi, T., Olafsson, J., Goddard, J. G., Chipman, D. W., and Sutherland, S. C.: Seasonal Variation of CO_2 and Nutrients in the High-Latitude Surface Oceans: a Comparative Study, Global Biogeochemical Cycles, 7, 843-878; doi:810.1029/1093GB02263, 1993.

Takahashi, T., Sutherland, S. C., Sweeney, C., Poisson, A., Metzl, N., Tilbrook, B., Bates, N. R., Wanninkhof, R., Feely, R. A., Sabine, C. L., Olafsson, J., and Nojiri, Y.: Global sea-air CO_2 flux based on climatological surface ocean pCO_2, and seasonal biological and temperature effects, Deep-Sea Research II, 49, 1601-1622, 2002.